JOURNAL OF CATALYSIS 114, 58–70 (1988)

# Europium-Exchanged Synthetic Faujasite Zeolites: A Luminescence Spectroscopic Study

JOHN R. BARTLETT,[1,*] RALPH P. COONEY,[2,†] AND RONALD A. KYDD‡

*Department of Chemistry, University of Newcastle, Newcastle, NSW 2308, Australia; †Department of Chemistry, University of Auckland, Private Bag, Auckland, New Zealand; and ‡Department of Chemistry, University of Calgary, 2500 University Drive, NW Calgary, Alberta T2N 1N4, Canada

Received May 15, 1987; revised May 31, 1988

A series of thermally activated europium-exchanged X and Y zeolites have been characterized by luminescence spectroscopy. The distribution of Eu(III) species has been deduced for both EuX and EuY samples (held at 20 K), on the basis of the observed $^5D_0 \rightarrow {}^7F_0$ luminescence emissions. For thermally activated EuY, only site $S_{I'}$ was found to be occupied by Eu(III) cations. In contrast, Eu(III) species were found to be distributed between sites $S_{I'}$ and $S_{II}$ in thermally activated samples of EuX. The effects of Eu(III) hydrolysis on the observed luminescence spectra are also discussed. © 1988 Academic Press, Inc.

## INTRODUCTION

Synthetic faujasite zeolites exchanged with rare earth cations are widely used in industry as cracking catalysts (*1*). In addition to conferring unusual thermal stability on the zeolite framework, the rare earth cations undergo a series of hydrolytic reactions during preparation (*2*), which results in the formation of framework and extra-framework hydroxyl species. Europium-exchanged zeolites in particular have been investigated by a wide range of techniques, including Mössbauer (*3–7*), electron paramagnetic resonance (*7–9*), and luminescence spectroscopy (*7, 10–14*). Additional rare earth ion-exchanged ($RE^{3+}$) faujasite zeolites have also been examined by various physicochemical techniques, including X-ray crystallography and neutron diffraction (*15–21*).

Luminescence spectroscopy has proven to be a particularly effective technique for the investigation of oxide surfaces incorporating Eu(III) species. Arakawa and coworkers (*11–13*) have made extensive use of the technique during their studies of the reactions between Eu(III) species and zeolitic water at temperatures in excess of 570 K *in vacuo*. These results and additional related studies have led to the development of a cyclic process based on EuY for the production of $H_2$ and $O_2$ from the thermolysis of water (*22*). Measurements of the lifetimes of Eu(III) luminescence emissions have also been employed to examine the coordination environment of hydrated and partially dehydrated Eu(III) species in various zeolite frameworks (*7, 14*).

The characteristic term diagram of the $Eu^{3+}$ ion is illustrated in Fig. 1. The emissions of interest in the present study arise from formally forbidden transitions between the $4f$ orbitals of the $Eu^{3+}$ ion. Since $4f$ orbitals are generally well shielded from the surrounding environment and are not involved in bonding to a significant extent, the energies of the individual $4f$ levels of $Eu^{3+}$ in a crystal or ligand field are comparable to those of the free ion (*23, 24*). As a consequence, the associated emission bands tend to appear at characteristic

[1] Permanent address: Materials Division, Australian Nuclear Science and Technology Organisation, Private Mail Bag 1, Menai, NSW 2234, Australia.

[2] Author to whom correspondence should be addressed.



0021-9517/88 $3.00
Copyright © 1988 by Academic Press, Inc.
All rights of reproduction in any form reserved.

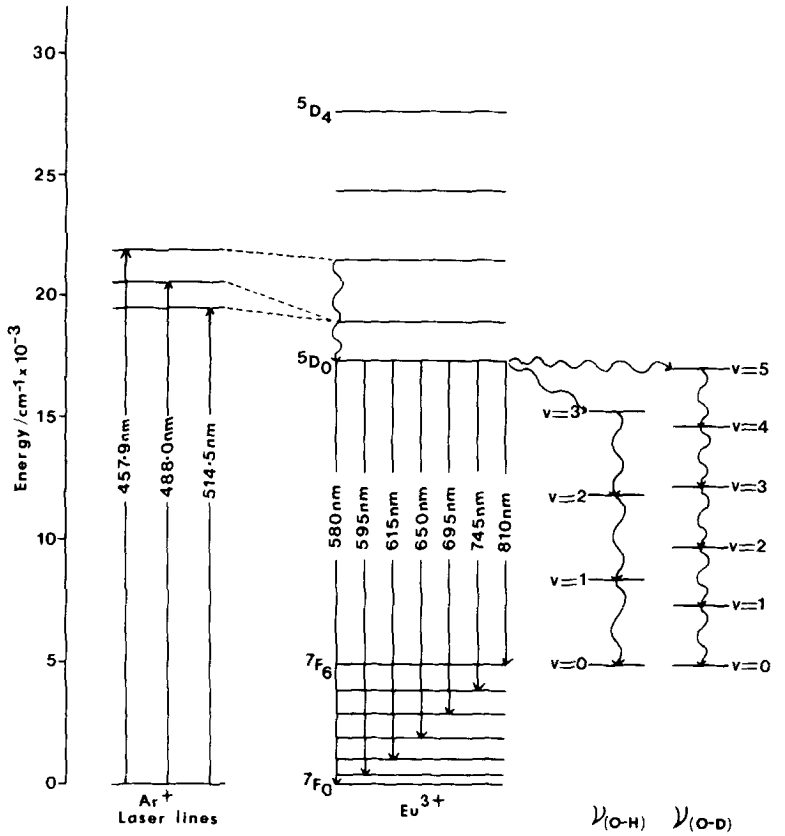


FIG. 1. Characteristic energy level diagram for the $Eu^{3+}$ ion, including the wavelengths of exciting lines employed in this study and the effects of coordinated water molecules.

wavelengths, as shown in Table 1 (see the Discussion for a more detailed account of $Eu^{3+}$ luminescence theory). One of the principal advantages of luminescence spectroscopy in studies of Eu(III) compounds is the ability of the technique to distinguish between differing environments for the Eu(III) species. This versatility stems from the fact that both the $^5D_0$ and $^7F_0$ terms of $Eu^{3+}$ are nondegenerate, regardless of the crystal or ligand field environment of the cation [Table 1 and Refs. (*23*, *24*)]. Consequently, the observation of multiple $^5D_0 \rightarrow {}^7F_0$ ($0 \rightarrow 0$) emissions provides direct spectroscopic evidence for the presence of multiple Eu(III) sites within the matrix. Brittain and Perry (*25*) have exploited this property to study the site distribution of Eu(III) species in $Eu_2O_3$ following various pretreatments.

Rare earth cations occupying sites in the internal channels of faujasite zeolites, unlike those in the sites of a conventional nonporous ionic lattice, are prone to reaction with such species as $H_2O$ and $CO_2$. Such potential side reactions would be expected to contribute to the complexity and breadth of luminescence spectra obtained from EuX and EuY samples. The role of associated water or hydroxyl species is particularly important (*23*), since the presence of such species within the first coordination sphere of Eu(III) ions provides an efficient mechanism for the vibrational relaxation of the emitting $^5D_0$ level (see the Discussion). This effect has been found to influence the relative intensities of emission bands associated with Eu(III)-exchanged mordenite as the amount of zeolitic water was varied by dehydration (*26*).

TABLE 1

Spectroscopic Properties of the $Eu^{3+}$ Ion, Including Wavelengths and Maximum Degeneracies of Commonly Observed Emission Bands

| Transition | Characteristics of emitted radiation | | Maximum number of observed bands for a single Eu(III) species |
|---|---|---|---|
| | nm | $cm^{-1}$ | |
| $^5D_0 \rightarrow {}^7F_0$ | 580 | 17,250 | 1 |
| $^5D_0 \rightarrow {}^7F_1$ | 595 | 16,800 | 3 |
| $^5D_0 \rightarrow {}^7F_2$ | 615 | 16,200 | 5 |
| $^5D_0 \rightarrow {}^7F_3$ | 650 | 15,370 | 7 |
| $^5D_0 \rightarrow {}^7F_4$ | 695 | 14,380 | 9 |
| $^5D_0 \rightarrow {}^7F_5$ | 745 | 13,440 | 11 |
| $^5D_0 \rightarrow {}^7F_6$ | 810 | 12,380 | 13 |

In the present study, we employ luminescence spectroscopy to examine the distribution of Eu(III) species in samples of EuX and EuY that have been dehydrated and reoxidized in oxygen at elevated temperatures. We also examine the influence of cation hydrolysis on the observed luminescence spectra, thus extending our earlier infrared investigation of Eu(III) hydrolysis in EuX zeolites (*2*).

## EXPERIMENTAL

*Sample preparation.* The preparation and composition of the samples referred to in this study as EuX-0.35, EuX-3.5, and EuX-18 have been described earlier (*2*). These zeolites exhibited comparable metal ion loadings, and are distinguished on the basis of the duration of the ion-exchange procedure used to prepare the individual samples (*2*). As an example, the sample labeled EuX-18 was ion-exchanged for 18 h. An additional EuX sample was also prepared by stirring a small sample of EuX-18 in dilute perchloric acid (ca. 0.02 mol/$dm^3$) for ca. 48 h. The resulting acid-washed sample is referred to as EuX-18/AW in subsequent discussion. A sample of EuY was also prepared according to the procedure previously employed during the preparation of EuX samples (*2*), with the exception that the parent NaY sample was not washed in dilute NaCl prior to buffer treatment and subsequent ion exchange. The compositions of both EuX-18/AW and EuY are included in Table 2.

Prior to use in luminescence experiments, the zeolites were activated [as described earlier (*2*)] in vials constructed from thin-walled 5-mm glass tubes connected to a conventional glass high-vacuum system. The samples were then cooled to room temperature, and permanently sealed under helium gas (99.99% purity, ca. 6–25 kPa).

*Equipment and techniques.* Luminescence spectra were recorded on a Jarrel-Ash double-stage monochromator equipped with an ITT Model FW130 photomultiplier. The spectrometer was interfaced to a microcomputer, which controlled all aspects of data acquisition and permitted routine smoothing and baseline correction of recorded spectra to be performed. Luminescence spectra were generally excited using the 514.5-nm line of a Coherent Radiation argon ion laser (100–200 mW), although some spectra were also recorded using the 488.0- and 457.9-nm lines. The spectral bandpass employed was generally within the range 5–10 $cm^{-1}$, although some spectra were recorded at a bandpass of 1 $cm^{-1}$ in an attempt to resolve fine structure on some of the bands.

All luminescence spectra reported in this paper were recorded from samples maintained at 20 K within the sample block of a Cryogenic Technology Inc. Model 20 closed-cycle helium cryostat. The interface between the sealed sample vials and the cryostat was lined with indium foil to maximize the dissipation of heat generated during exposure of the samples to high levels of radiant flux. Spectra were also acquired from unactivated samples cooled to 20 K to ensure the absence of surface contaminants such as $EuCl_3$ (from the original exchange procedure) and $Eu(OH)_3$ [which could form within the zeolite channels in the event of extensive Eu(III) hydrolysis (*27*)].

X-ray diffraction patterns of EuX-18/AW

TABLE 2

Conditions Used to Prepare Europium-Exchanged Zeolites, Including Analyses, Surface Areas, and Unit Cell Parameters[a]

| Zeolite code | Eu:Na charge equivalents in initial exchange medium | Exchange time (h) | Nominal surface area ($m^2\ g^{-1}$) | Unit cell (nm) | Composition[b] |
|---|---|---|---|---|---|
| EuX-18/AW | 4.5 | 18 | Not measured | 2.493 | $Na_{18}Eu_{17}X$ |
| EuY | 6.8 | 19 | 848 | 2.470 | $Na_{14}Eu_{11}Y$ |

[a] Analyses for Na and Eu calculated on the basis of neutron activation and semiquantitative EDAX data. Analyses for Al and Si calculated on the basis of EDAX data only.
[b] $X = (AlO_2)_{79}(SiO_2)_{113}$. $Y = (AlO_2)_{49}(SiO_2)_{143}$.

and EuY were also obtained, and the calculated unit cell parameters are included in Table 2. Both samples exhibited sharp, well-defined reflections, in accord with the retention of a high degree of crystallinity following sample preparation. The unit cell dimensions of EuX-18/AW (2.493 ± 0.002 nm) were slightly lower than those of EuX-18 (2.502 ± 0.002 nm) and NaX (2.501 ± 0.002 nm), possibly reflecting minor leaching of framework aluminum during acid washing. The unit cell parameter of EuY (2.470 ± 0.002) was comparable to that of the parent NaY sample (2.473 ± 0.002 nm). The nominal surface area of the EuY sample examined in this study was found (*2*) to be (850 ± 5%) $m^2/g$, which is slightly higher than the value of 789 $m^2/g$ previously reported by Eberly and Kimberlin (*28*) for europium-exchanged synthetic faujasite.

## RESULTS

The luminescence spectra observed for activated samples of EuX-0.35, EuX-18, EuX-18/AW, and EuY at 20 K (using 514.5 nm excitation) are shown in Figs. 2–5. The $0 \rightarrow 0$ and $0 \rightarrow 1$ emission profiles for the various EuX samples and for EuY are illustrated in Figs. 2 and 3, respectively, while the corresponding $0 \rightarrow 2$ emission profiles are included in Figs. 4 and 5, respectively. The spectrum of EuX-18 was also excited with 488.0- and 457.9-nm radiation in sepa-

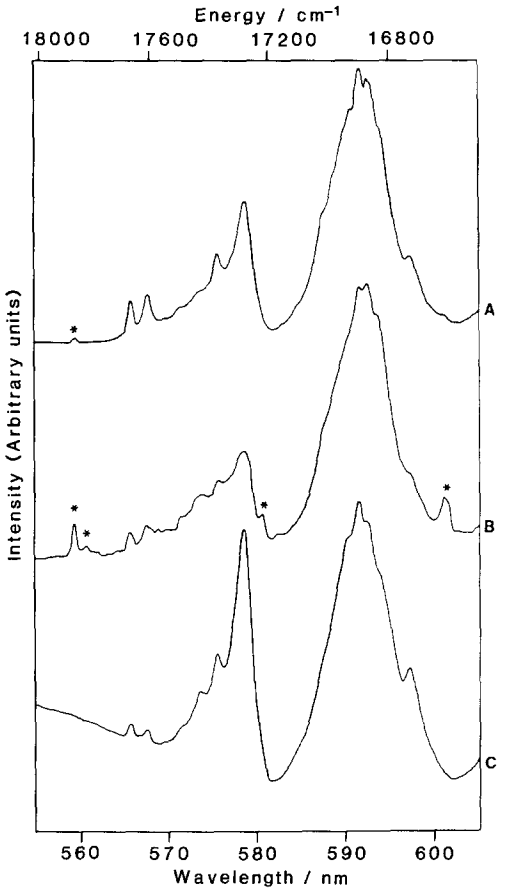


FIG. 2. $^5D_0 \rightarrow {}^7F_0$ and $^5D_0 \rightarrow {}^7F_1$ emission profiles of activated EuX zeolites. (A) EuX-0.35. (B) EuX-18. (C) EuX-18/AW. Top and bottom traces: 10 $cm^{-1}$ bandpass, 100 mW, 514.5-nm exciting line; middle trace: 6 $cm^{-1}$ bandpass, 150 mW, 514.5-nm exciting line. All spectra were recorded at 20 K. Bands marked with an asterisk are artifacts.

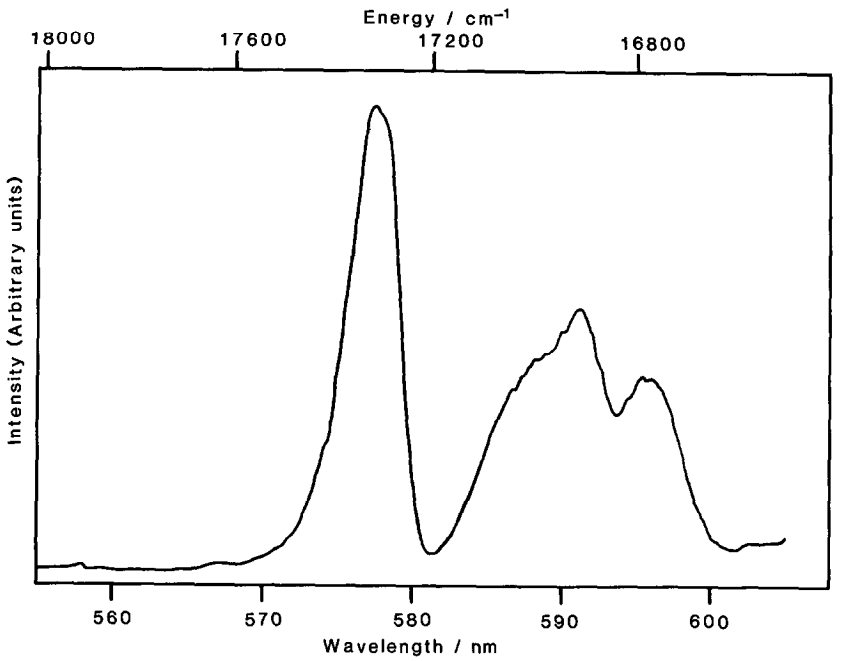


FIG. 3. $^5D_0 \rightarrow {}^7F_0$ and $^5D_0 \rightarrow {}^7F_1$ emission profiles of activated EuY zeolite. 10 $cm^{-1}$ bandpass, 100 mW, 514.5-nm exciting line. Spectrum recorded at 20 K.

rate experiments to confirm that none of the observed bands were associated with vibrational modes of the sample. Emission spectra excited with 457.9-nm radiation exhibited a signal-to-noise ratio (S/N) comparable to that of spectra recorded using 514.5-nm excitation. In contrast, the S/N of spectra recorded using 488.0-nm excitation was significantly poorer. This phenomenon is a consequence of the fact that the 457.9- and 514.5-nm lines are in near resonance with the Eu(III) $^5D_2$ and $^5D_1$ terms, respectively, while the 488.0-nm line does not overlap with any levels of the $^5D$ manifold (Fig. 1).

The wavelengths and proposed assignments of the various emission bands observed in this study are summarized in Table 3. Assignments are based on the energy level scheme shown in Fig. 6 (see below). The assignment of bands in the spectral region 570–580 nm for the EuX zeolites is complicated by overlap of emissions associated with $^5D_1 \rightarrow {}^7F_2$ ($1 \rightarrow 2$) and $^5D_0 \rightarrow {}^7F_0$ ($0 \rightarrow 0$) transitions. The strategy employed in formulating band assignments and deriving the energy level schemes illustrated in Fig. 6 involved postulating the minimum number of distinct Eu(III) species that is consistent with the emission profiles observed above 580 nm. In the cases of EuX-0.35, EuX-3.5, EuX-18, and EuX-18/AW, at least two nonequivalent Eu(III) species are required to account for the observed $0 \rightarrow 2$ emission profile, which exhibits seven separate bands ($Eu^{3+}$ cations residing in a single site can give rise to a maximum of five $0 \rightarrow 2$ bands, Table 1). As a consequence, at least two of the bands observed in the region 570–580 nm in Fig. 2 are necessarily associated with $0 \rightarrow 0$ transitions, while the remaining bands may be assigned to $1 \rightarrow 2$ transitions.

In this study, it has been found that an internally consistent description of the various EuX spectra may be obtained by locating $^5D_1$ terms at 18,669 and 18,612 $cm^{-1}$, and $^5D_0$ terms at 17,286 and 17,376 $cm^{-1}$, as illustrated in Fig. 6. The energies of the various $^5D_2$ levels may then be obtained from

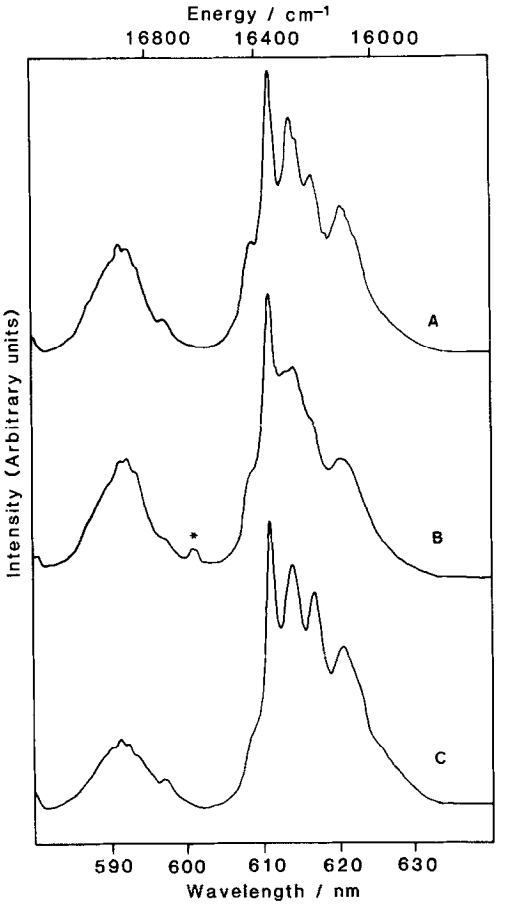


FIG. 4. $^5D_0 \rightarrow {}^7F_1$ and $^5D_0 \rightarrow {}^7F_2$ emission profiles of activated EuX zeolites. (A) EuX-0.35. (B) EuX-18. (C) EuX-18/AW. Conditions as for Fig. 2.

the known energies of the $0 \rightarrow 2$ transitions (Fig. 4 and Table 3). The bands at 565.8, 567.7, 571.6, and 573.4 nm (Fig. 2) are subsequently assigned to $1 \rightarrow 2$ emissions, while the additional bands at 575.5 and 578.5 nm are attributed to $0 \rightarrow 0$ emissions. Since the degeneracy of the Eu(III) $0 \rightarrow 0$ transition is always unity, regardless of the environment of the cation, the observation of two $0 \rightarrow 0$ transitions indicates that Eu(III) cations in activated samples of EuX reside in two distinct environments. The additional weak features observed in the spectra of Fig. 2 at 559.4, 561.0, 580.5, and 601.1 nm (labeled with an asterisk) are thought to be experimental artifacts, since they were not observed in spectra excited with 457.9-nm radiation.

The region 570–580 nm in the spectrum of EuX-18/AW was also investigated by subband analysis, and the calculated band profiles are illustrated in Fig. 7. The weak feature found at 577 nm during this analysis (Fig. 7), if authentic, probably arises from one of two possible $1 \rightarrow 2$ transitions at ca. 575 nm, which were predicted on the basis of Fig. 6. Such a transition originating in a $^5D_1$ level would be expected to be of low intensity relative to transitions originating in $^5D_0$ levels (*23*).

## DISCUSSION

### A. Emission Spectroscopy and Energy Levels of the $Eu^{3+}$ Cation

The emission spectrum of $Eu^{3+}$ has been found (*26*) to constitute a sensitive probe of

TABLE 3

Observed Band Positions (nm) and Assignments for the Luminescence Spectra of Activated EuX and EuY

| EuY | EuX-0.35 | EuX-3.5 | EuX-18 | EuX-18/AW | Assignment |
|---|---|---|---|---|---|
| | 565.8 | 565.6 | 565.7 | 565.6 | |
| | 567.7 | 567.5 | 567.6 | 567.5 | $^5D_1 \rightarrow {}^7F_2$ |
| | 571.6 | 571.2 | 571.5 | 571.6 | |
| | 573.4 | 573.4 | 573.5 | 573.7 | |
| | 575.5 | 575.4 | 575.7 | 575.5 | |
| 577.6 | 578.5 | 578.4 | 578.5 | 578.4 | $^5D_0 \rightarrow {}^7F_0$ |
| 588.5 | | | | | |
| | 590.3 | 590.3 | 590.2 | 590.2 | |
| 591.1 | 591.5 | 591.4 | 591.4 | 591.3 | $^5D_0 \rightarrow {}^7F_1$ |
| | 592.3 | 592.3 | 592.3 | 592.2 | |
| 595.7 | 597.0 | 597.2 | 597.0 | 597.1 | |
| | 608.9 | 608.9 | 608.9 | 608.9 | |
| | 611.3 | 611.1 | 610.9 | 611.2 | |
| 612.9 | 613.9 | 613.9 | 614.1 | 613.9 | $^5D_0 \rightarrow {}^7F_2$ |
| | 616.8 | 616.8 | 616.6 | 616.8 | |
| 620.3 | 620.6 | 620.6 | 620.7 | 620.6 | |
| | ca. 622 | ca. 622 | ca. 622 | ca. 622 | |
| 625.2 | ca. 624 | ca. 624 | ca. 624 | ca. 624 | |
| 645.3 | | | | | |
| 648.5 | 649.6 | 649.4 | 649.4 | 649.4 | |
| 654.8 | 654.7 | 654.2 | | 654.2 | $^5D_0 \rightarrow {}^7F_3$ |
| | 656.7 | 655.9 | 655.6 | 656.3 | |
| 657.4 | 657.8 | 657.7 | 657.8 | 675.5 | |
| 681.7 | | | | | |
| 682.2 | 683.2 | 682.2 | 681.1 | 682.3 | |
| 684.0 | 685.9 | 685.7 | 685.4 | 685.6 | |
| 689.0 | 688.6 | 688.5 | 688.1 | 689.2 | |
| 691.8 | 691.9 | 691.7 | 691.7 | 691.9 | $^5D_0 \rightarrow {}^7F_4$ |
| | 696.0 | 695.5 | | 695.5 | |
| 702.0 | | | | | |
| | 703.8 | 703.8 | 703.4 | 703.6 | |
| 705.7 | 706.7 | 706.6 | 706.1 | 706.6 | |
| | 711.2 | 711.0 | 710.9 | 711.0 | |

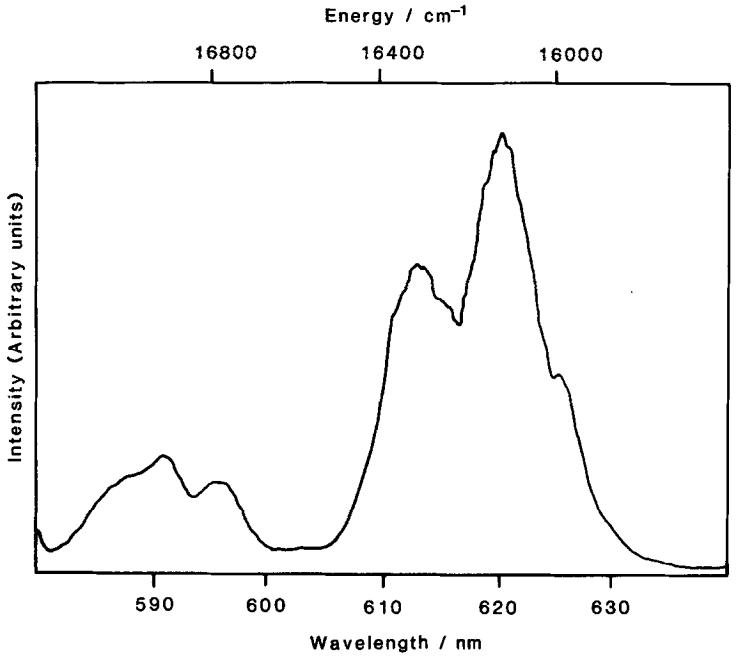


FIG. 5. $^5D_0 \rightarrow {}^7F_1$ and $^5D_0 \rightarrow {}^7F_2$ emission profiles of activated EuY zeolite. Conditions as for Fig. 3.

the structural environment surrounding the cation. The emissions of interest are those involving transitions between the $4f$ orbitals of the $Eu^{3+}$ ion (*23, 24, 29, 33*). Since such transitions are formally forbidden, they give rise to relatively weak spectra in both emission and absorption (*23*). A complete discussion of lanthanide $f$–$f$ intensities and associated selection rules may be found in Ref. (*29*). Since $4f$ orbitals are generally well shielded from the surrounding environment and are not involved in bonding to a significant extent, the energies of the individual $4f$ levels of $Eu^{3+}$ in a crystal or ligand field are comparable to those of the free ion. As a consequence, the associated emission bands tend to appear at characteristic wavelengths, as summarized in Table 1.

The characteristic term diagram of the $Eu^{3+}$ ion is shown in Fig. 1. The $^7F_J$ (ground state) and $^5D_J$ (excited state) manifolds are split by the large magnitude of the spin–orbit coupling, and the various $^7F_J$ levels in particular may be separated by hundreds of wavenumbers (Fig. 1). Transitions from the $^5D_0$ level to the $^7F_{0,1,2}$ levels are usually the most easily observed, and excitation into levels higher than $^5D_0$ generally results in efficient population of the $^5D_0$ level (Fig. 1). The individual free ion levels are $(2J + 1)$-fold degenerate as illustrated in Table 1, and this degeneracy may be lifted to an extent depending on the point symmetry of the environment surrounding the $Eu^{3+}$ ion. Of particular importance are that levels for which $J = 0$ are nondegenerate, and, consequently, the observation of more than one $0 \rightarrow 0$ transition in the Eu(III) emission spectrum constitutes direct spectroscopic evidence for the existence of nonequivalent Eu(III) cation sites.

The intensities of Eu(III) $f$–$f$ emissions are also influenced by a range of nonradiative relaxation processes. One of the most important examples of this effect involves energy transfer from the $^5D_0$ level to the ground state via overlap with the vibrational manifold of coordinated water molecules or hydroxyl groups. This effect is illustrated in Fig. 1. The efficiency of vibrational relaxation processes is heavily

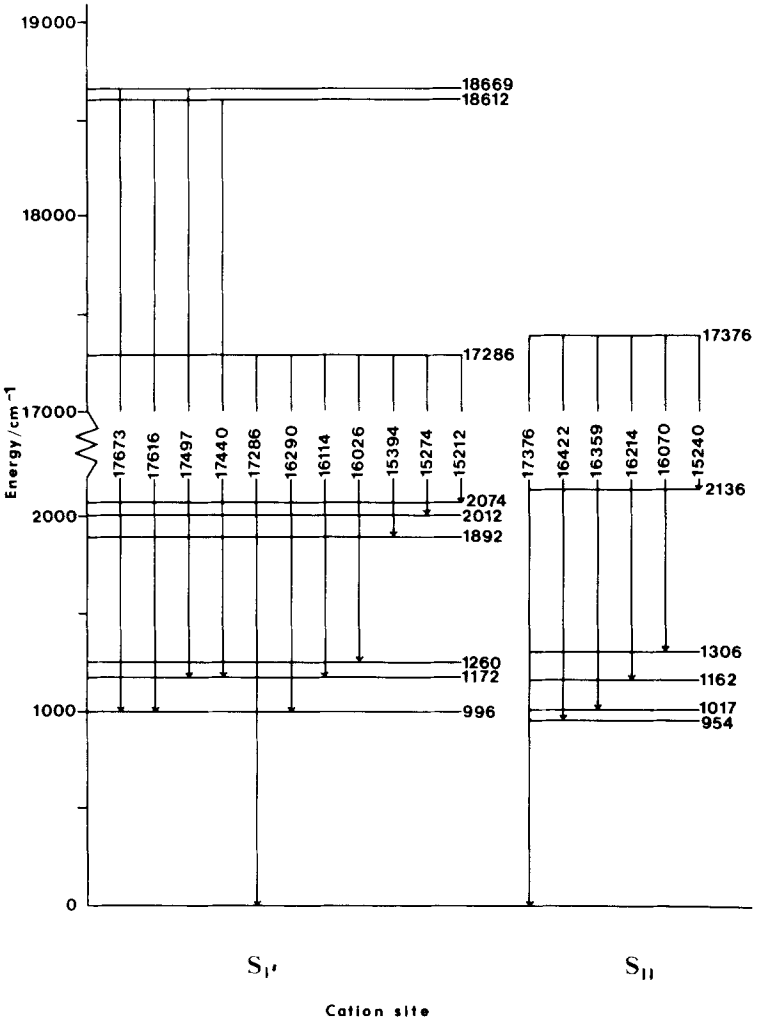


FIG. 6. Proposed energy level scheme and band assignments for Eu(III) species in $S_{I'}$ and $S_{II}$. $0 \rightarrow 1$ and $0 \rightarrow 4$ transitions are not included. Energy levels have been calculated from the spectrum of EuX-0.35 (Table 3).

influenced by the ease with which the energy gap between the emissive level ($^5D_0$) and the highest level of the electronic ground state manifold ($^7F_6$) can be bridged by the vibrational manifold of the coordinating ligand. For this reason, coordinated $H_2O$ molecules provide a much more efficient relaxation mechanism than, say, $D_2O$, since in the former case, relaxation proceeds via the third overtone, while in the latter case, it proceeds via the fourth or fifth overtone.

## B. $0 \rightarrow 0$ Transitions and Site Counting

### *Activated EuX Zeolites*

*Effects of europium(III) hydrolysis on luminescence spectra.* The intensities of the $0 \rightarrow 0$ emission profiles of EuX-0.35, EuX-18, and EuX-18/AW vary in a systematic manner with respect to the associated $0 \rightarrow 1$ emission profiles in Fig. 2. The decreasing relative intensity of the $0 \rightarrow 0$ profile as we progress from EuX-0.35 to EuX-18 (Figs.

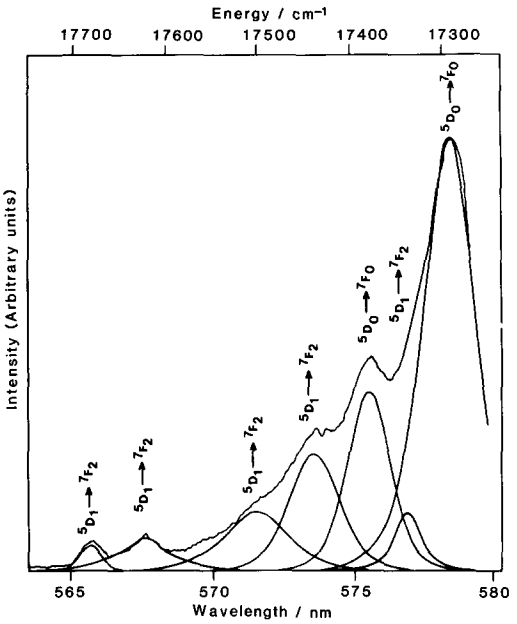


FIG. 7. Sub-band analysis, including proposed band assignments, of overlapping band profiles (570–580 nm) in the spectrum of EuX-18/AW.

2A and B) follows the trend toward increasing extent of Eu(III) hydrolysis previously identified during infrared spectroscopic charaterization of these materials (*2*). The role of Eu(III) hydrolysis in mediating the observed changes in relative intensity may be further assessed by an examination of the spectrum of EuX-18/AW (Fig. 2C). Acid washing of EuX-18 (see Experimental) would be expected to reduce the extent of Eu(III) hydrolysis by promoting the back reaction

$$Eu(OH)^{2+} + H^+ \rightarrow Eu^{3+} + H_2O.$$

The relative intensity of the $0 \rightarrow 0$ emission profile in the spectrum of EuX-18/AW is significantly greater than that of either EuX-0.35 or EuX-18 (Fig. 2), suggesting that cation hydrolysis directly influences relative $0 \rightarrow 0$ band intensities.

The influence of cation hydrolysis on the observed emission spectra may be associated with vibronic interactions between coordinated hydroxyl species and the $Eu^{3+}$ ion, as illustrated earlier in Fig. 1 (see earlier discussion). The vibrational manifold of the –OH oscillator efficiently bridges the energy gap between the emitting level ($^5D_0$) and the $^7F_6$ level of the $Eu^{3+}$ ion, providing a facile pathway for vibrational relaxation of the excited ion. Increasing Eu(III) hydrolysis would thus be expected to be accompanied by an increase in the efficiency of vibrationally coupled relaxation of the excited state, since hydrolysis results in an increasing abundance of hydroxyl species in intimate contact with the ion (*2*).

If the relative intensities of luminescence emission are considered to reflect the probability that radiative decay of the $^5D_0$ level will occur via a given radiative transition, then increasing competition from an additional nonradiative mechanism would be expected to influence the intensity of formally forbidden transitions [e.g., $0 \rightarrow 0$; see Ref. (*29*)] to a greater extent than formally allowed transitions (e.g., $0 \rightarrow 1$). Consequently, increasing Eu(III) hydrolysis may be expected to result in decreasing relative intensity of the $0 \rightarrow 0$ emission band, as observed in Fig. 2. Related effects have been reported by Arakawa *et al.* (*26*) during their studies of the dehydration of europium-exchanged mordenite zeolites.

*Origin of multiple europium(III) environments.* Eu(III) cations in activated EuX appear to reside in at least two distinct environments, as discussed earlier. The nonequivalence of these sites may be related either to the effects of cation hydrolysis or to cation–framework interactions, and as a consequence, two explanations for the observed data have been considered. The first interpretation would require that the discrete $0 \rightarrow 0$ emissions arise from Eu(III) species in nonequivalent zeolite cation sites (e.g., $S_I$, $S_{I'}$, $S_{II}$, etc.), while the full width at half-maximum (FWHM) of the observed bands is influenced by the distribution of hydrolyzed species present at each site. The second interpretation associates the individual $0 \rightarrow 0$ emissions with nonequivalent or discrete hydrolysis products, while the FWHM of observed bands is

influenced by the number of zeolite cation sites occupied by the discrete Eu(III) species.

Our selection of the first interpretation as the preferred model is based on the following aspects of the data obtained in this study:

(i) The observation that the relative intensities of bands constituting the $0 \rightarrow 0$ emission profile do not change substantially with increasing extent of cation hydrolysis provides the most compelling evidence in favor of the first model (see spectra of EuX-0.35 and EuX-18/AW in Figs. 2A and C). Specifically, if the bands at 575.5 and 578.5 nm were associated with distinct hydrolysis products, then significant variations in their relative intensities would be anticipated with increasing hydrolysis of the Eu(III) cations.

(ii) Bands constituting the $0 \rightarrow 0$ emission profile of EuX-18 (Fig. 2B) are somewhat broader than those of either EuX-0.35 (Fig. 2A) or EuX-18/AW (Fig. 2C). The increasing FWHM correlates with increases in the extent of Eu(III) hydrolysis, consistent with the first model proposed above.

It is thus concluded that the observation of two $0 \rightarrow 0$ transitions is consistent with Eu(III) species residing in two crystallographically distinct cation sites in the case of EuX samples.

*Activated EuY Zeolites*

The spectrum of EuY over the range 560–600 nm is shown in Fig. 3. The observation of a single $0 \rightarrow 0$ emission band at 577.6 nm (Table 3) suggests that Eu(III) species reside in a single cation site in the EuY sample investigated in this study, in contrast to the cation distribution previously deduced for EuX. A recent crystallographic investigation of activated LaY with a comparable rare earth cation loading (67% exchanged) has also found that the rare earth cations reside in a single site, viz., $S_{I'}$ in this latter case (*16*).

The relative intensity of the $0 \rightarrow 0$ emission band associated with EuY is substantially greater than that observed for either EuX-0.35 or EuX-18, and is also somewhat greater than that associated with EuX-18/AW (Fig. 2). These observations suggest that vibrational relaxation of the Eu(III) $^5D_0$ level is less efficient in EuY than in the various samples of EuX examined, suggesting that the Eu(III) species are not as extensively hydrolyzed in EuY. This conclusion is in accord with the expected behavior of multivalent cations in synthetic faujasites (*15*). Our recent studies of U(VI) speciation within the same zeolite frameworks (*30*) have also suggested that the interchannel basicity of Y zeolites was lower than that of X zeolites.

The influence of cation–framework interactions in determining the energies of Eu(III) $0 \rightarrow 0$ transitions is also illustrated by a comparison of the spectra of EuY and the various samples of EuX (Table 3). The wavelength of the $0 \rightarrow 0$ emission associated with EuY (577.6 nm) is approximately equal to that of the dominant peak in the $0 \rightarrow 0$ emission profile of EuX (ca. 578.5 nm), suggesting that the bands arise from Eu(III) species in a common cation site. The additional bands associated with EuY (arising from $0 \rightarrow 1$ and $0 \rightarrow 2$ transitions) also have close counterparts in the spectra of the various EuX samples (Table 3). These observations confirm that the framework environment surrounding the various Eu(III) species plays a decisive role in determining the energies of the various emissions observed.

### C. $0 \rightarrow 1$ and $0 \rightarrow 2$ Transitions in Activated EuX and EuY

The $0 \rightarrow 1$ emission profiles associated with EuX and EuY are included in Figs. 2 and 3, respectively. The band profiles observed for samples of EuX (centered at ca. 590 nm) were generally found to be broad and featureless. In contrast, the $0 \rightarrow 1$ emission profile associated with EuY exhibits three broad overlapping bands with maxima at 588.5, 591.1, and 595.7 nm. This is the maximum number of $0 \rightarrow 1$ components

that can arise from a discrete Eu(III) emitter, because the degeneracy of the $^7F_1$ level of the free ion is 3 (Table 1). This result is entirely consistent with our earlier conclusion (based on an analysis of the $0 \rightarrow 0$ emissions) that Eu(III) species in EuY reside in a single cation site, and is indicative of the low symmetry of the environment surrounding the Eu(III) species in this latter zeolite (*23*).

The emission spectra of EuX-0.35, EuX-18, and EuX-18/AW from 580 to 640 nm are included in Fig. 4. This region of the spectrum is dominated by the $0 \rightarrow 2$ emission profile, which, for distinct Eu(III) species, may consist of up to five discrete bands (Table 1). The $0 \rightarrow 2$ emission profiles illustrated in Fig. 4 each exhibit seven broad components, with maxima at 608.9, 611.3, 613.9, 616.8, 620.6, ca. 622, and ca. 625 nm (Table 3). This result confirms our earlier finding, namely that Eu(III) species must occupy at least two distinct cation sites in the EuX samples investigated in this study. The increasing extent of Eu(III) hydrolysis in the case of EuX-18 (see earlier discussion) is also reflected in the increasing FWHM of bands constituting the $0 \rightarrow 2$ emission profile in this latter case (Fig. 4B).

The $0 \rightarrow 2$ emission profile of EuY (Fig. 5) is somewhat simpler than that associated with the various EuX samples. Two relatively strong bands may be distinguished in Fig. 5, with maxima at 612.9 and 620.3 nm. An additional shoulder is also observed at ca. 625–626 nm. These findings are in accord with our earlier conclusion that Eu(III) cations in EuY reside in a single site, and further suggest that the symmetry of the environment surrounding the rare earth cations must be less than tetragonal (*23*).

### D. Assignment of Observed Emissions to Cation Sites

An extension to the previous discussion involves elucidating the discrete crystallographic sites actually occupied by Eu(III) species in activated EuX and EuY. A number of earlier workers have examined the structures of related synthetic faujasite zeolites incorporating $La^{3+}$ and $Ce^{3+}$ cations (*15–21*). The distribution of cations within these materials would be expected to be comparable to those of EuX and EuY.

A recent crystallographic investigation of the cation distribution in dehydrated LaY (*16*) located all La(III) species in site $S_{I'}$ within the sodalite cage. Since activated EuY is also characterized by Eu(III) species residing in a single cation site, it follows that the Eu(III) species in this latter case also reside in site $S_{I'}$. Earlier crystallographic studies of dehydrated CeX and LaX (*15, 20, 21*) have concluded that the rare earth ions in these latter materials were distributed among sites $S_I$, $S_{I'}$, and $S_{II}$. Since the dominant $0 \rightarrow 0$ emission observed for EuX (at 578.5 nm) appears at approximately the same energy as the single $0 \rightarrow 0$ emission associated with EuY, the 578.5-nm band of EuX is also presumably associated with Eu(III) cations residing in site $S_{I'}$.

An assignment of the additional $0 \rightarrow 0$ emission at 575.5 nm (associated with EuX samples; see Table 3 and Fig. 2) to a specific cation site is somewhat speculative, since the band may be associated with Eu(III) species in either $S_I$ or $S_{II}$. However, an earlier study of Eu(III) species in silicate glasses (*31*) has associated decreasing $0 \rightarrow 0$ transition energy with an increase in the strength of the Eu(III)–lattice interaction. On this basis, the 575.5-nm band may be assigned to Eu(III) species residing in $S_{II}$. This assignment is based on the expectation that cations residing in the sodalite cage (i.e., $S_{I'}$ cations) would be perturbed by the zeolite framework to a greater extent than cations protruding into the supercage (i.e., $S_{II}$ cations). The observation of a band at 1445 $cm^{-1}$ in the infrared spectrum of pyridine adsorbed on EuX, which appears to be associated with the formation of an Eu(III):pyridine complex (*32*), is also in accord with the above assignment, since pyri-

dine can only coordinate to cations protruding into the supercage.

A self-consistent energy level diagram characterizing Eu(III) species in the various cation sites identified above is presented in Fig. 6. The strategy employed during the construction of this diagram has been described earlier (see Results). Since all bands observed for EuY appear to be associated with cations residing in site $S_{I'}$, corresponding bands observed in the spectra of EuX samples may also be assigned to $S_{I'}$ cations. Additional bands observed in the spectra of samples of EuX which have no counterparts in the spectrum of EuY may then be assigned to $S_{II}$ cations, since these latter species are not present in EuY. Transitions to the $^7F_1$ level have been neglected in the above analysis, due to the broad and featureless nature of the observed $0 \rightarrow 1$ emission profile in the case of EuX samples.

A final aspect of the emission spectra concerns the observation that although $1 \rightarrow 2$ emissions were observed for all EuX samples examined at 20 K, no corresponding bands could be detected for EuY. Emissions from the $^5D_1$ level are generally observed with very low intensity in the luminescence spectra of Eu(III) species, since the level is rapidly depopulated by vibrational relaxation to the $^5D_0$ level via coupling with vibrations of the host lattice (*23*). This latter observation suggests that increasing interactions between the host lattice and Eu(III) species may be accompanied by a reduction in the intensity of emissions from the $^5D_1$ level. Consequently, the absence of such emissions in the spectrum of EuY (Fig. 3) may occur as a result of stronger interactions between the framework and the Eu(III) species in the case of EuY, as compared to EuX.

## ACKNOWLEDGMENTS

We thank the Natural Sciences and Engineering Research Council of Canada for the equipment used during this study. Helpful discussions with Dr. T. Dines are gratefully acknowledged. One of us (J.R.B.) also acknowledges financial assistance in the form of an Australian Commonwealth Postgraduate Research Student Award.

## REFERENCES

1. Wallace, D. N., *Amer. Chem. Soc. Symp. Ser.* **164,** 101 (1981).
2. Bartlett, J. R., Kydd, R. A., and Cooney, R. P., *J. Catal.* **114,** 53 (1988).
3. Suib, S. L., Zerger, R. P., Stucky, G. D., Emberson, R. M., Debrunner, P. G., and Iton, L. E., *Inorg. Chem.* **19,** 1858 (1980).
4. Samuel, E. A., and Delgass, W. N., *J. Chem. Phys.* **62,** 1590 (1975).
5. Delgass, W. N., and Samuel, E. A., *Amer. Chem. Soc. Div. Petrol. Chem. Prepr.* **17,** C52–C60 (1972).
6. Samuel, E. A., *Chem. Abstr.* **83,** 68622Y (1975).
7. Stucky, G. D., Iton, L. E., Morrison, T. I., Shenoy, G. K., Suib, S. L., and Zerger, R. P., *J. Mol. Catal.* **27,** 71 (1984).
8. Iton, L. E., and Turkevich, J., *J. Phys. Chem.* **81,** 435 (1977).
9. Nicula, A., and Turkevich, J., *Rev. Roum. Phys.* **76,** 2325 (1974).
10. Buechler, E., and Turkevich, J., *J. Phys. Chem.* **76,** 2325 (1972).
11. Arakawa, T., Takata, T., Adachi, G. Y., and Shiokawa, J., *J. Lumin.* **20,** 325 (1979).
12. Arakawa, T., Takata, T., Adachi, G. Y., and Shiokawa, J., *J. Chem. Soc. Chem. Commun.*, 453 (1979).
13. Arakawa, T., Takata, T., Takakuwa, M., Adachi, G. Y., and Shiokawa, J., *Mater. Res. Bull.* **17,** 171 (1982).
14. Suib, S. L., Zerger, R. P., Stucky, G. D., Morrison, T. I., and Shenoy, G. K., *J. Chem. Phys.* **80,** 2203 (1984).
15. Breck, D. W., "Zeolite Molecular Sieves: Structure, Chemistry, and Use," Chap. 6 (and references therein). Wiley, New York, 1974.
16. Cheetham, A. K., Eddy, M. M., and Thomas, J. M., *J. Chem. Soc. Chem. Commun.*, 1337 (1984).
17. Olson, D. H., Kokotailo, G. T., and Charnell, J. F., *Nature (London)* **215,** 270 (1967).
18. Olson, D. H., Kokotailo, G. T., and Charnell, J. F., *J. Colloid Interface Sci.* **28,** 305 (1968).
19. Smith, J. V., Bennett, J. M., and Flanigen, E. M., *Nature (London)* **215,** 241 (1967).
20. Hunter, F. D., and Scherzer, J., *J. Catal.* **20,** 246 (1971).
21. Bennett, J. M., Smith, J. V., and Angell, C. L., *Mater. Res. Bull.* **4,** 77 (1969).
22. Kasai, P. H., and Bishop, R. J., Jr., U.S. Patent 3,963,830 (1976).
23. Horrocks, W. W., Jr., and Albin, M., *Prog. Inorg. Chem.* **31,** 1 (1984) and references therein.
24. Dieke, G. H., *in* "Spectra and Energy Levels of Rare Earth Ions in Crystals" (H. M. Crosswhite

and H. Crosswhite, Eds.). Interscience, New York, 1968.
25. Brittain, H. G., and Perry, D. L., *J. Catal.* **77,** 94 (1982).
26. Arakawa, T., Takakuwa, M., Adachi, G. Y., and Shiokawa, J., *Bull. Chem. Soc. Japan* **57,** 1290 (1984).
27. Baes, C. F., Jr., and Mesmer, R. E., "The Hydrolysis of Cations," Chap. 7, p. 129. Wiley, New York, 1976.
28. Eberly, P. E., Jr., and Kimberlin, C. N., Jr., *in* "Advances in Chemistry Series" (R. F. Gould, Ed.), Vol. 102, p. 374. Amer. Chem. Soc., Washington, DC, 1971.
29. Peacock, R. D., *Struct. Bonding* **22,** 83 (1975).
30. Bartlett, J. R., and Cooney, R. P., submitted.
31. Kurkjian, C. R., Gallagher, P. L., Sinclair, W. R., and Sigety, E. A., *Phys. Chem. Glass* **4,** 239 (1963).
32. Ward, J. W., *J. Catal.* **14,** 365 (1969).
33. Carnall, W. T., *in* "Handbook on the Physics and Chemistry of Rare Earths" (K. A. Gschneider, Jr., and L. Eyring, Eds.), Vol. 3, Ch. 24. North-Holland, Amsterdam, 1979.